# Cyclogenetic Perturbations and Analysis Errors Decomposed into Singular Vectors

CHRIS SNYDER

*National Center for Atmospheric Research, Boulder, Colorado*

GREGORY J. HAKIM

*Department of Atmospheric Sciences, University of Washington, Seattle, Washington*

(Manuscript received 5 January 2004, in final form 12 November 2004)

ABSTRACT

Singular vectors (SVs) have been applied to cyclogenesis, to initializing ensemble forecasts, and in predictability studies. Ideally, the calculation of the SVs would employ the analysis error covariance norm at the initial time or, in the case of cyclogenesis, a norm based on the statistics of initial perturbations, but the energy norm is often used as a more practical substitute.

To illustrate the roles of the choice of norm and the vertical structure of initial perturbations, an upper-level wave with no potential vorticity perturbation in the troposphere is considered as a typical cyclogenetic perturbation or analysis error, and this perturbation is then decomposed by its projection onto each energy SV. All calculations are made, for simplicity, in the context of the quasigeostrophic Eady model (i.e., for a background flow with constant vertical shear and horizontal temperature gradient). Viewed in terms of the energy SVs, the smooth vertical structure of the typical perturbation, as well as its evolution, results from strong cancellation between the growing and decaying SVs, most of which are highly structured and tilted in the vertical.

A simpler picture, involving less cancellation, follows from decomposition of the typical perturbation into SVs using an alternative initial norm, which is based on the relation between initial norms and the statistics of initial perturbations together with the empirical assumption that the initial perturbations are not dominated by interior potential vorticity. Differences between the energy SVs and those based on the alternative initial norm can be understood by noting that the energy norm implicitly assumes initial perturbations with second-order statistics given by the covariance matrix whose inverse defines the energy norm. Unlike the "typical" perturbation, perturbations with those statistics have large variance of potential vorticity in the troposphere and fine vertical structure.

Finally, a brief assessment is presented of the extent to which the upper wave, and more generally the alternative initial norm, is representative of cyclogenetic perturbations and analysis errors. There is substantial evidence supporting deep perturbations with little vertical structure as frequent precursors to cyclogenesis, but surrogates for analysis errors are less conclusive: operational midlatitude analysis differences have vertical structure similar to that of the perturbations implied by the energy norm, while short-range forecast errors and analysis errors from assimilation experiments with simulated observations are more consistent with the alternative norm.

## 1. Introduction

Singular vectors (SVs) are the perturbations that, under dynamics linearized about a basic flow, grow most rapidly over a given time interval and in a given measure of amplitude, or norm. These optimal perturbations have been posited as explanations for midlatitude cyclogenesis (Farrell 1989) and have been applied to forecast error growth and ensemble forecasting (Lorenz 1965; Lacarra and Talagrand 1988; Farrell 1990; Buizza et al. 1993). In this paper, we project typical cyclogenetic perturbations and analysis errors onto SVs and examine two issues that arise: the relation of the SVs to the dynamics of the typical perturbations and the choice of norm for the SVs. For both conceptual and narrative simplicity, our calculations use the quasigeostrophic equations and the basic state of Eady (1949).

Problems of cyclogenesis and forecast-error growth are similar in that they both involve, to a first approximation, the linear evolution over a finite time interval of small perturbations (or errors) about a known basic state. The SVs are the natural tools in such problems and have several appealing properties. Because the SVs are orthogonal, the growth of a perturbation can be

*Corresponding author address:* Dr. Chris Snyder, National Center for Atmospheric Research, P.O. Box 3000, Boulder, CO 80307-3000.
E-mail: chriss@ucar.edu

calculated by summing over the SVs. One consequence of this fact is that any perturbation exhibiting net amplification over the time interval must project (using the inner product that defines the chosen norm) onto at least one of the growing SVs; that is, projection onto the growing SVs is a necessary condition for growth. The SVs are also well defined for basic states with arbitrary space and time dependence, for which modal solutions based on separation of variables may not exist. In addition, the singular values (the amplifications of the SVs) in many systems are large for only a few leading SVs. The growth of perturbations can then be approximated by projecting onto the low-dimensional subspace spanned by those leading SVs (e.g., Gelaro et al. 1998). Further background on SVs is given in section 2.

Since both problems involve evolution over a finite time interval, the characteristics of the initial conditions must be relevant to some degree. To state this somewhat differently, the results of both problems depend not only on the evolution of perturbations or errors, but also on the typical characteristics of the initial perturbations or errors. Our fundamental goal will be to explore how the vertical structure of the initial perturbations enters the SV calculation. We will consider two related, and more specific, issues as avenues toward this goal.

First, the leading SVs for commonly used norms such as energy most often, though not invariably, possess distinctive vertical structure, with amplitude concentrated in the mid to lower troposphere and strong vertical tilts against the basic-state shear. The SV dynamics are also distinctive and involve in part the untilting or unshielding of perturbation potential vorticity under advection by the shear (Hoskins et al. 2000; Kim and Morgan 2002). This is not the usual picture of cyclogenesis, nor is it clear that forecast errors evolve in this manner. Thus, we ask how the dynamics of typical perturbations relate to those of the leading SVs.

Second, the SVs require the choice of a norm. It is well known that SV structure and amplifications depend, sometimes strongly, on this choice (Palmer et al. 1998; Snyder and Joly 1998). In principle, the preferred initial norm is related to the covariance matrix of the initial perturbations (Houtekamer 1995; Ehrendorfer and Tribbia 1997; Palmer et al. 1998; Barkmeijer et al. 1998). This norm measures, in a sense that will be made more precise in section 5, the likelihood of an initial perturbation and therefore penalizes "atypical" perturbations. We will thus ask how the preferred covariance norm differs from the most commonly used norm, the total energy, which Palmer et al. (1998) suggest as a first approximation to the analysis-error covariance norm. We will also suggest an empirical alternative to the energy norm and examine the perturbations implied by the energy norm using the relation between a norm and the covariance matrix for the initial perturbations.

Our starting point in addressing these issues will be to consider an example in which a typical perturbation is decomposed into SVs. The results of the example of course hinge on what we take to be a typical perturbation; here, we choose an upper trough above a straight surface baroclinic zone. This choice is hardly controversial for midlatitude cyclogenesis, as it is perhaps the most familiar cyclogenetic initial condition. The situation is less clear for analysis errors. What information exists on the statistics of analysis errors comes from imperfect surrogates, such as short-range forecast errors or analysis differences, and is not conclusive. The upper trough here is consistent with some of that information, as will be discussed in section 7.

The outline of the paper is as follows. Model equations are given in section 2, followed by a precise definition of the SVs and a brief discussion of their structure and dynamics for the Eady basic state in section 3. In section 4, we decompose the upper trough above a surface baroclinic zone into SVs. The evolution of this perturbation is easily understood in terms of potential vorticity and its associated induced flows (e.g., Hoskins et al. 1985), yet in terms of SVs, the evolution is a complex superposition of rapidly growing and decaying perturbations, each of which exhibits dynamics distinct from that of the original upper trough. Section 5 reviews norms based on covariance matrices, which are the natural initial norm when the statistics of initial perturbations are known, and presents an empirical covariance norm based on the notion that typical perturbations have only limited potential vorticity in the interior of the troposphere. Singular vectors for this initial norm provide a particularly simple representation for the upper trough. Section 6, which also begins from the relation of norms and covariance matrices, considers the initial perturbations implied by the total energy norm. We then argue in section 7 that our chosen typical perturbation, the upper trough, is broadly representative of both typical cyclogenetic perturbations and is consistent with some surrogates for analysis errors. Section 8 provides a summary of our results.

## 2. Formulation

Our starting point is the equation describing the quasigeostrophic evolution of perturbations to a zonal flow with constant vertical shear $\Lambda$ and uniform interior potential vorticity confined between rigid boundaries at $z = 0, H$ (i.e., the Eady problem; see Gill 1982). Taking $N$ to be the Brunt–Väisälä frequency and $f$ to be the Coriolis parameter, we nondimensionalize height by $H$, horizontal distance by $NH/f$ and horizontal velocities by $\Lambda H$. If we consider, for simplicity, solutions in which the streamfunction has the form $\phi(z, t)\exp(ikx)$, the governing equation is then

$$[\partial_t + ik(z - 1/2)]q = 0, \tag{1a}$$

with boundary conditions

$$[\partial_t + ik(z - 1/2)]\theta - ik\phi = 0 \quad \text{at } z = 0, 1, \quad (1b)$$

where $q = (\partial_{zz} - k^2)\phi$ is the pseudopotential vorticity (PV), $\theta = \phi_z$ is the potential temperature perturbation, and we have assumed that the basic-state zonal wind, $z - 1/2$, is zero at the midlevel of the domain.

Discretizing in the vertical and seeking modal solutions $\boldsymbol{\phi}(t) = \exp(\omega t)\mathbf{e}$, (1) can be written as the eigenvalue problem

$$\mathbf{Ae} = \alpha\mathbf{Be},$$

where $\mathbf{A}$, $\mathbf{B}$ are matrices that depend on $k$ and the vertical discretization, and $\boldsymbol{\phi}$ is a vector containing the streamfunction at each grid level. The calculations here will use centered second-order differences and $n$ grid points staggered with respect to $z = 0, 1$, as described in more detail in the appendix. The resulting eigenvectors correspond to the modes of the Eady problem: $n - 2$ are analogs of the continuous spectrum modes and the remaining two are a conjugate pair of growing/decaying modes for $k < k_c$ or a pair of counter propagating neutral modes for $k > k_c$ (where $k_c \approx 2.4$; again, see Gill 1982).

Let $\mathbf{E}$ be the matrix whose columns are the eigenvectors of (1), and let $\boldsymbol{\alpha}$ be the vector of modal projection coefficients for an arbitrary initial condition, that is $\boldsymbol{\phi}(0) = \mathbf{E}\boldsymbol{\alpha}$. Then $\boldsymbol{\phi}$ evolves according to

$$\boldsymbol{\phi}(t) = \mathbf{M}(t)\boldsymbol{\phi}(0), \quad (2)$$

where

$$\mathbf{M}(t) = \mathbf{E}\Omega(t)\mathbf{X}^*,$$

$\boldsymbol{\Omega}(t)$ is diagonal with entries $\exp(\omega_j t)$, $\mathbf{X}$ has as columns the adjoint eigenvectors normalized so that $\mathbf{X}^*\mathbf{E} = \mathbf{I}$, and stars denote the conjugate transpose.

## 3. Energy singular vectors for the Eady basic state

The SVs depend on a time interval ($[0, \tau]$, say) and a choice of norm. If we define an inner product $(\mathbf{x}, \mathbf{y}) = \mathbf{x}^*\mathbf{Sy}$ and a norm $|\mathbf{x}| = (\mathbf{x}, \mathbf{x})^{1/2}$, with $\mathbf{S}$ a symmetric, positive definite matrix, the SVs of $\mathbf{M} = \mathbf{M}(\tau)$ are the eigenvectors of

$$\mathbf{S}^{-1}\mathbf{M}^*\mathbf{SMu} = \sigma^2\mathbf{u}. \quad (3)$$

The singular values of $\mathbf{M}$ are the corresponding values of $\sigma$, the square root of the eigenvalues. In what follows, the SVs are assumed normalized such that $|\mathbf{u}_i| = 1$ and ordered such that $\sigma_1 \geq \sigma_2 \geq \cdots \geq \sigma_n$. Results shown in this section use the volume-integrated total energy as norm, in which case $\mathbf{S}$ is the discretized form of $k^2 - \partial_{zz}$ (see appendix), but qualitatively similar results are obtained for the squared streamfunction norm. Initial norms based on the covariance matrix of the initial perturbations are considered in section 5.

The SVs have two properties that make them a convenient basis for describing the growth of perturbations, particularly over a limited time interval. First, the singular values give the amplification of each SV over the time interval $[0, \tau]$: $|\mathbf{Mu}_i| = \sigma_i|\mathbf{u}_i|$. Second, the SVs are orthogonal and their orthogonality is maintained even after evolution to $t = \tau$: $(\mathbf{u}_i, \mathbf{u}_j) = \delta_{ij}$ and $(\mathbf{Mu}_i, \mathbf{Mu}_j) = \sigma_i^2\delta_{ij}$. For derivations and further details see, for example, Buizza et al. (1993).

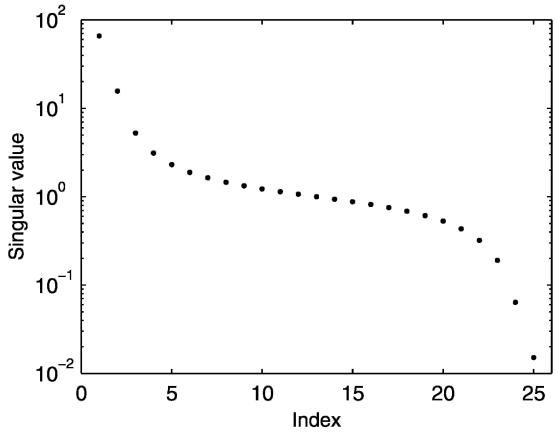


FIG. 1. Singular values ($\sigma_i$) of $\mathbf{M}$ for $n = 25$, $k = 2.5$, and $\tau = 5$.

To see why these properties are useful, let us consider an arbitrary initial condition, $\boldsymbol{\phi}(0)$, and its decomposition into the SVs, $\boldsymbol{\phi}(0) = \Sigma\ \alpha_i\mathbf{u}_i$ where $\alpha_i = (\boldsymbol{\phi}(0), \mathbf{u}_i)$. The initial magnitude of the perturbation, $|\boldsymbol{\phi}(0)|$, is then the square root of the sum of the squares of the projection coefficients $\alpha_i$. Moreover, the magnitude of the perturbation at $t = \tau$ is

$$|\boldsymbol{\phi}(\tau)|^2 = |\mathbf{M}\boldsymbol{\phi}(0)|^2 = \sum \sigma_i^2|\alpha_i|^2.$$

Thus, knowing the initial projection coefficients, we can compute the squared norm of the evolved $\boldsymbol{\phi}(\tau)$ by simply weighting the square of each projection coefficient $\alpha_i$ by square of the corresponding singular value.

These results have the important consequence that any initial perturbation that grows on $[0, \tau]$ must project, using the inner product defined by $\mathbf{S}$, on the subset of SVs that grow (i.e., which have $\sigma_i > 1$). Thus, projection on the growing SVs is a necessary condition for perturbation growth. For nonorthogonal bases such as the modal solutions (the eigenvectors of $\mathbf{M}$), there is not a simple relation between the projection coefficients and the norm at either initial or final time; perturbations can grow even though they do not project on unstable modes (Farrell 1989). In addition, if only a few leading singular values are large, the evolution of $\boldsymbol{\phi}(0)$ can be approximated by retaining the projection only onto those leading SVs. An example of this property, which is often used in predictability studies (such as Gelaro et al. 1998), appears in the next section.

Singular values for the Eady basic state are shown in Fig. 1 for $n = 25$ vertical points, horizontal wavenumber

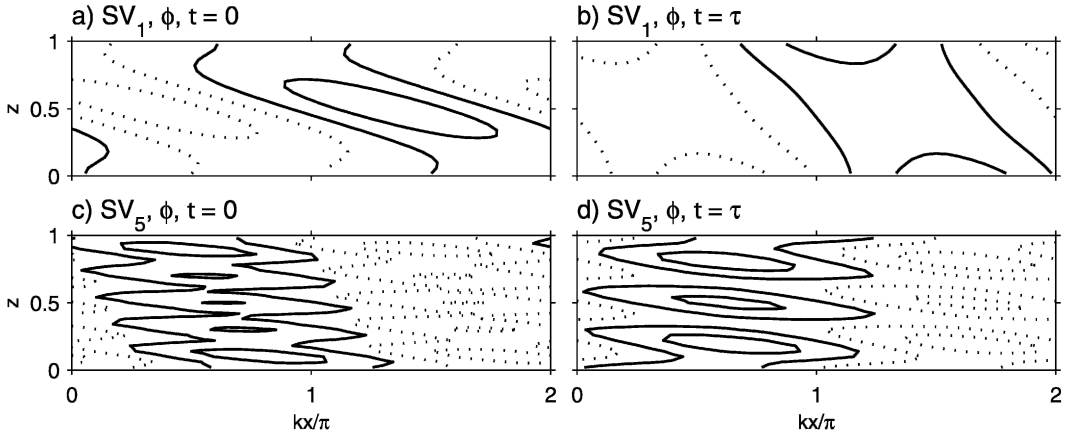


FIG. 2. The first and fifth energy SVs. Streamfunction at $t = 0$: (a) Re($e^{ikx}\mathbf{u}_1$) and (c) Re($e^{ikx}\mathbf{u}_5$). Streamfunction at $t = \tau$: (b) Re($e^{ikx}\mathbf{M}\mathbf{u}_1$) and (d) Re($e^{ikx}\mathbf{M}\mathbf{u}_5$). Contour values are 1/4 and 3/4 of the (arbitrary) maximum in (a) and (c), and increase by factors of 14 and 1.7 in (b) and (d), respectively. Negative values are shown in dashed lines.

$k = 2.5$, and a time interval of length $\tau = 5$. In terms of dimensional quantities, these correspond to a wavelength of $2.5 \times 10^3$ km and a time interval of 2 days for the parameter values $\Lambda = 3 \times 10^{-3}$ m s$^{-1}$, $N = 10^{-2}$ s$^{-1}$, $H = 10$ km, and $f = 10^{-4}$ s$^{-1}$. Although at this wavenumber all the modes are neutral, the energy of the leading SV amplifies by a factor of 66 from $t = 0$ to $t = \tau$.

The first and fifth SVs ($\mathbf{u}_1$ and $\mathbf{u}_5$) for the Eady basic state, and their evolved structure, are shown in Fig. 2. The leading SV at $t = 0$ (Fig. 2a) tilts strongly westward with height, against the shear of the basic flow, especially in the midtroposphere. This vertical structure in $\phi$ arises from anomalies of potential vorticity for $0 < z < 1$ (not shown), which have very nearly the form of a plane wave in $z$; the SV has only weak potential temperature anomalies at the boundaries $z = 0, 1$ and these cause the modulation of the plane wave structure in $\phi$ near the boundaries. Mukogawa and Ikeda (1994) and Morgan (2001) provide further discussion of the leading SV for the Eady problem, including its dependence on $\tau$.

As is now familiar from numerous studies, the evolution of the SV is characterized by the steady reduction of its vertical tilt, as its potential vorticity is advected and "tipped over" by the basic-state shear according to (1a); at the end of the time interval ($t = \tau$, Fig. 2b), the vertical tilt of the SV has decreased, the magnitude of the boundary temperature anomalies has increased relative to that of the interior potential vorticity, and the midtropospheric structure is smooth.

The intermediate growing SVs ($\mathbf{u}_2, \ldots, \mathbf{u}_{12}$) have similar structure and evolution, of which the fifth SV shown in Figs. 2c,d is an example. Each has progressively more vertical structure and stronger westward tilt, this tilt is associated with interior PV of approximately plane wave form and, as the SV evolves, the tilt decreases with time.

Conversely, the decaying SVs ($\mathbf{u}_{14}, \ldots, \mathbf{u}_{25}$) tilt eastward with height and their tilt increases with time. In fact, the last, and most rapidly decaying, SV can be inferred from Fig. 2; its initial structure is given by reflecting Fig. 2b (i.e., the leading SV at $t = \tau$) about $z = 1/2$ and its structure at $t = \tau$ is given by the same reflection of Fig. 2a (the leading SV at $t = 0$).[1] The structure of $\mathbf{u}_{21}$ can be inferred in a similar manner from Figs. 1c,d.

## 4. Growing perturbations decomposed into SVs

A common initial condition for cyclogenesis is an upper trough passing above an undisturbed surface baroclinic zone. We will argue in section 7 that analysis errors may also resemble this initial perturbation in certain qualitative respects. A simple explanation for the growth of such a perturbation is given by Hoskins et al. (1985). Associated with the upper trough, there are surface southerlies to the east of the trough axis, leading to the development of a surface warm anomaly to the east of the upper trough. The disturbance thus tilts westward with height and begins a phase of growth and surface deepening. How does this scenario appear when interpreted in terms of SVs?

A simple version of this initial condition is

$$q = 0, \quad \text{for} \quad 0 < z < 1; \quad \phi_z = \begin{cases} 0, & z = 0 \\ 1, & z = 1 \end{cases}. \qquad (4)$$

We choose a zonal wavenumber $k = 2.5$, somewhat beyond the short-wave cutoff for the unstable Eady

[1] The governing equations (1) are unchanged if $t$ is replaced by $-t$ and $x$ by $-x$ since there is no dissipation and the basic state is steady and zonal. Because of this symmetry, $\mathbf{M}^{-1}$ is the complex conjugate of $\mathbf{M}$, $\mathbf{u}_{n-i}$ is (aside from a normalization) the conjugate of $\mathbf{M}\,\mathbf{u}_i$, and, as shown in Fig. 1, $\sigma_{n-i} = 1/\sigma_i$.

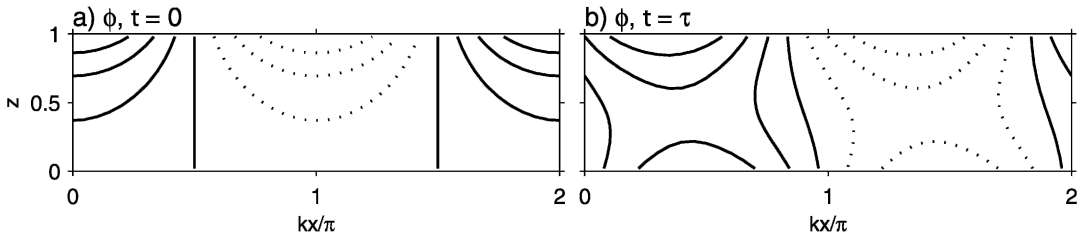


FIG. 3. Streamfunction $\phi$ at (a) $t = 0$, corresponding to the initial condition (4), and at (b) $t = \tau$. The contour interval is 0.25 and negative values are dashed.

modes. The upper trough is represented by the potential temperature perturbation at the upper boundary, and there is no surface disturbance (in $\theta$); the full solution for streamfunction [i.e., $\mathrm{Re}(\phi \exp(ikx))$] is shown in Fig. 3a. A more general initial condition might include interior PV associated with the upper trough; this possibility is discussed below. By $t = \tau$ (Fig. 3b), the disturbance has developed a westward tilt with height and the surface pressure perturbation has strengthened by more than a factor of 5.

Although all the eigenmodes of $\mathbf{M}$ are stable at $k = 2.5$, the disturbance energy doubles over the same interval. Rotunno and Fantini (1989) examine the growth of similar initial conditions in terms of superposition of the neutral eigenmodes. Here, we consider how that growth appears in terms of the energy SVs.

Figure 4 shows the modulus of the SV projection coefficients, $|\alpha_i|$. The perturbation (4) projects significantly on the leading, growing SVs, although the largest projections occur for the last three (decaying) SVs. Also shown in Fig. 4 are the projection coefficients of the evolved perturbation $\boldsymbol{\phi}(\tau)$ onto the orthonormal basis defined by the evolved SVs. (The basis vectors are $\mathbf{v}_i = \mathbf{M}\,\mathbf{u}_i/\sigma_i$.) This illustrates how retaining just a few leading SVs can provide a reasonable approximation to $\boldsymbol{\phi}(\tau)$: the first four SVs grow rapidly enough to account for over 90% of the perturbation energy at $t = \tau$ even though they account for less than 10% of the initial energy.

The projection at the initial time in Fig. 4, with largest projection on the last two SVs and a broad projection on the other SVs, appears to be closely related to qualitative differences in vertical structure between our chosen disturbance and the majority of SVs. The SVs all possess vertical structure on finer scales than the disturbance and only the last two SVs have maxima (in streamfunction) on the boundaries. The disturbance therefore projects a little on many SVs and more strongly on the trailing SVs.

A related point is that representing the disturbance as a sum of SVs requires much mutual cancellation among the terms in the sum. The disturbance PV exemplifies this point, as the disturbance has $q = 0$ initially and for all subsequent times [because of the conservation of $q$ expressed by (1a)]. The SVs, on the other hand, each possess interior PV, which must cancel in the sum. Figure 5, which shows the partial sums $\Sigma_{i=1}^{m} \alpha_i \mathbf{u}_i$, $m = 1, 5, 20, 24, n$ for both streamfunction and PV, illustrates how this cancellation is accomplished. The first few SVs contribute PV that tilts westward with height. Adding additional growing SVs to the sum increases the vertical structure. When the decaying SVs are added, the vertical structure of the PV begins to decrease until the addition of the final few decaying SVs cancels the PV completely. The westward tilt of the streamfunction, on the other hand, steadily decreases as more SVs are retained in the sum, and the vertical structure becomes steadily smoother.

It is important to emphasize that this cancellation (of potential vorticity) among the SVs does not in any way invalidate the use of the SVs to describe growth in the chosen norm. Indeed, the SVs are orthogonal and thus, by definition, do not suffer cancellation in the chosen norm. In terms of other quantities, however, the SVs are subject to cancellation, as shown in Fig. 5. Thus, while the SVs are a preferred basis for describing growth of perturbations in the chosen norm, decomposing in terms of SVs may yield a more complicated picture of other aspects of perturbation development, such as potential-vorticity dynamics.

We have also projected other initial conditions, including the most unstable normal mode and a disturbance similar to (4) but with a strong PV anomaly at

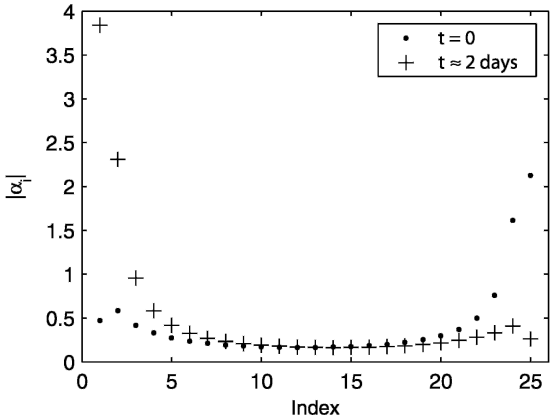


FIG. 4. Modulus of the projection coefficients $|\alpha_i|$ for the initial condition (4) onto the initial SVs (dots) and for the evolved perturbation $\boldsymbol{\phi}(\tau)$ onto the evolved SVs (crosses).

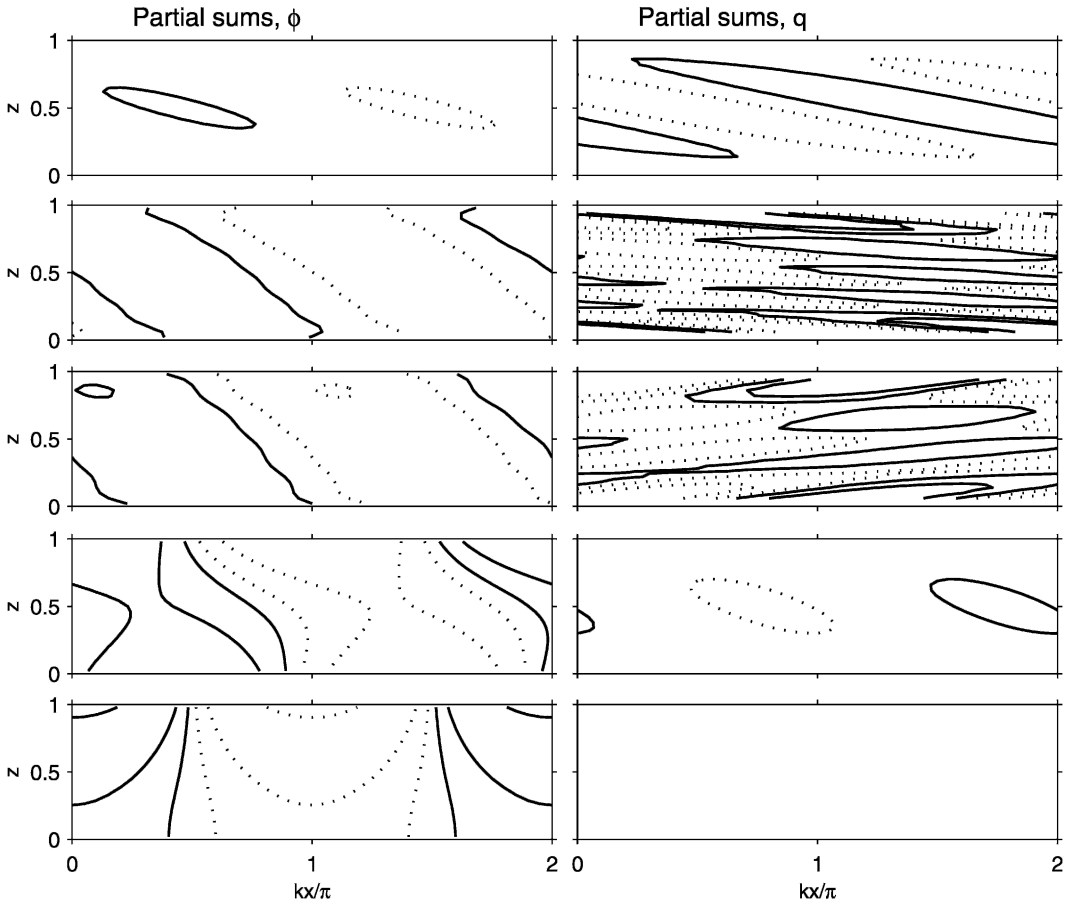


FIG. 5. The portion of the initial condition (4) given by the partial sum $\Sigma_{i=1}^{m} \alpha_i \mathbf{u}_i$. From top to bottom, rows show the partial sum for $m = 1, 5, 20, 24, n$, for (left) streamfunction and (right) interior PV. Contour values are $\pm 0.02$, $\pm 0.08$, $\pm 0.32$ for streamfunction and $\pm 0.5$, $\pm 2$, $\pm 8$ for PV, with negative values dashed. In the lowest panel at right, PV is identically zero.

upper levels, onto the SVs. Even for initial perturbations with nonzero PV, the most obvious perturbations based on synoptic experience do not resemble any of the SVs (though the vertical structure of analysis errors is less well known; see section 7). Including the gradient of the Coriolis parameter, and thus a nonzero gradient of the basic-state PV, in (1a) also has little effect on the results. Thus, in all these cases, the projection onto the SVs is qualitatively similar to that shown in Fig. 4 and the comments above, regarding both cancellation among SVs and dynamical interpretations, remain applicable.

Of course, there is a large class of initial perturbations for which cancellation of PV among the SVs is less severe and whose dynamics are more similar to that of the first few SVs—we can simply excite all the SVs equally (by drawing each $\alpha_i$ independently from identical probability distributions) or restrict $\alpha_i$ to be nonzero only for the leading SVs. But, as will be discussed in section 6, such perturbations differ qualitatively in their vertical structure from the upper trough given by (4). This leads us to consider in the next section how information about the structure of typical perturbations can be incorporated into the SV calculation.

## 5. An empirical covariance norm

Improving the correspondence between the SVs and the structure of typical initial perturbations requires an initial norm for the SVs that incorporates information about typical perturbation structure. Before specifying the norm, we must first define more precisely the characteristics of typical perturbations.

A useful way to do this is to suppose that the perturbations $\boldsymbol{\phi}$ are drawn randomly from a specified Gaussian probability distribution function (pdf) with mean 0 and covariance matrix $\mathbf{P}$ [or, in more abbreviated notation, $N(\mathbf{0}, \mathbf{P})$]. The probability density is then given by

$$p(\boldsymbol{\phi}) = (2\pi)^{-n/2}(\det\mathbf{P})^{-1/2} \exp\left(-\frac{1}{2}\boldsymbol{\phi}^{*}\mathbf{P}^{-1}\boldsymbol{\phi}\right). \quad (5)$$

Given $\mathbf{P}$, we can specify a norm that measures how likely, and thus how typical, an initial perturbation is.

The norm, which we will term a covariance norm, is given by

$$|\boldsymbol{\phi}|_0^2 = \boldsymbol{\phi}^* \mathbf{P}^{-1} \boldsymbol{\phi}, \tag{6}$$

where the subscript 0 indicates that the norm is to be evaluated at the initial time. Comparing (5) and (6) shows that the covariance norm is proportional to the negative logarithm of $p(\boldsymbol{\phi})$. Thus, the covariance norm directly relates to how likely an initial perturbation is; the smaller of two perturbations is more likely, and perturbations with equal norms have equal probability.

After choosing another norm for $t = \tau$, say $|\boldsymbol{\phi}|_\tau^2 = \boldsymbol{\phi}^* \mathbf{S} \boldsymbol{\phi}$, the SVs then satisfy

$$\mathbf{PM}^* \mathbf{SMu} = \sigma^2 \mathbf{u}. \tag{7}$$

If the SVs are meant to represent the evolution of analysis errors at $t = 0$ to forecast errors at $t = \tau$, then $\mathbf{P}$ should be the analysis error covariance matrix. In that case (and assuming linear evolution of the errors), evolving the leading singular vector to the forecast time and then scaling by $\mathbf{S}^{1/2}$ gives the leading eigenvector of the forecast-error covariance matrix as measured by the norm defined by $\mathbf{S}$. More precisely, if $\mathbf{u}$ is the leading singular vector of (7), then $\mathbf{S}^{1/2}\mathbf{Mu}$ is the leading eigenvector of $\mathbf{S}^{1/2}\mathbf{MPM}^*\mathbf{S}^{1/2}$. Further discussion of covariance norms and calculations of approximate analysis-error covariance SVs appear in Houtekamer (1995), Ehrendorfer and Tribbia (1997), Barkmeijer et al. (1998), Palmer et al. (1998), and Hamill et al. (2003).

Note that the singular value $\sigma$ in (7) is the ratio of the final norm to the initial norm and is not an amplification, as it would be if the initial and final norms were the same. Thus, perturbation growth does not enter directly in the definition of the SVs (though it can be implicit in $\mathbf{M}$). In particular, the leading SV does not maximize growth but rather maximizes $|\boldsymbol{\phi}(\tau)|_\tau$ over all equally likely $\boldsymbol{\phi}(0)$.

A basic feature of the upper trough that distinguishes it from (most of) the energy SVs is its smooth vertical structure. Let us assume for the moment that typical perturbations (both cyclogenetic perturbations and analysis errors) share the upper trough's lack of rapid variations in the troposphere. We next define an empirical covariance matrix, and thus an empirical covariance norm, that is consistent with perturbations having smooth vertical structure. Again, we will return in section 7 to the question of whether such vertical structure is representative of either cyclogenetic perturbations or analysis errors.

The streamfunction for this quasigeostrophic system may be computed, given $\theta$ at the surface and tropopause and PV in the interior troposphere. In the discretized problem, it is convenient to incorporate the boundary $\theta$ into a generalized PV at the first or last levels as discussed in the appendix. Vertical structure in the troposphere other than smooth decay away from the boundaries is then associated with PV at the other $n - 2$ interior levels. The upper-level trough given by (4), in particular, has zero interior PV.

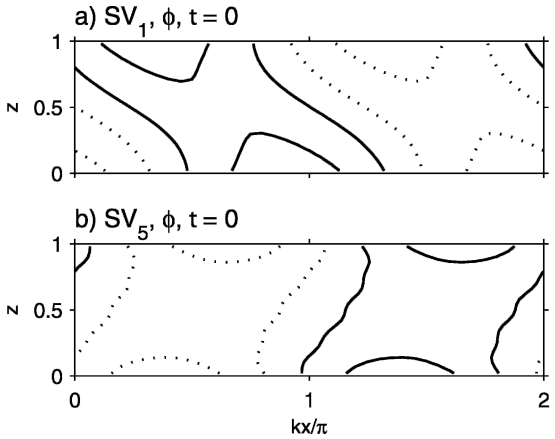


FIG. 6. As in Fig. 2 but for the first and fifth initial SVs in the empirical covariance norm given by (6) and (8).

Thus, to ensure that typical perturbations have little vertical structure, we assume that they have relatively little interior PV and take the PV variance summed over all $n - 2$ interior levels to be equal to the sum of the (generalized) PV variance at the first and last levels. (The precise ratio between the interior and boundary PV is not critical as long as the interior PV is not dominant.) For simplicity, we also assume that the PV variance is the same at each of those $n - 2$ interior levels and that the PV perturbations at each level are mutually independent.

When specified in this way, the covariance matrix $\mathbf{Q}$ for the PV perturbations is diagonal, and the covariance matrix for the streamfunction perturbations becomes

$$\mathbf{P} = \nabla^{-2} \mathbf{Q} \nabla^{-2}, \tag{8}$$

where $\nabla^{-2}$ is the inverse of the discretized Laplacian operator.

The SVs using this empirical covariance norm are then calculated using $\mathbf{P}$ in (7). The first and fifth SVs at initial time are shown in Fig. 6. Unlike the energy SVs (Fig. 2), the $\mathbf{P}$-norm SVs have deep vertical structure and modest vertical tilts; they are also qualitatively more similar to our chosen, typical perturbation (Fig. 3).

The amplitude of the projection of the typical perturbation onto the covariance SVs appears in Fig. 7, which may be compared with the energy SV projections in Fig. 4. For the covariance SVs, the projection is noticeably more broad at the initial time and is largest for roughly the first ten SVs. After the perturbation has evolved to $t = \tau$, the projection coefficients drop off even more steeply as the SV index increases. The steeper decrease of the projection means that project-

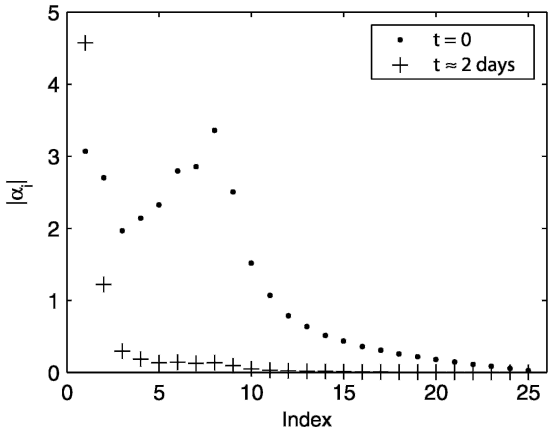


FIG. 7. As in Fig. 4 but for projections onto the empirical covariance SVs. The projection uses the inner product based on the inverse of the empirical covariance matrix at the initial time and the energy inner product at the final time.

ing onto just a few leading covariance SVs provides a better approximation to the initial upper trough and its evolution than would projection onto the same number of energy SVs.

Moreover, the covariance SVs provide a different view of the growth and evolution of the upper trough. Rather than emphasizing a small initial projection onto SVs that then grow rapidly and change their form greatly, the covariance SVs focus attention on perturbations associated with the tropopause and surface that grow more slowly and maintain their smooth vertical structure. Since their vertical structure is similar to that of our chosen upper trough throughout its evolution, the summation of covariance SVs is subject to less cancellation (in terms of both $\boldsymbol{\phi}$ and the PV) than the energy SVs.

## 6. Perturbations implied by the energy norm

The previous section examined the norm and associated SVs that follow from the assumption that the initial perturbations are random with covariance matrix $\mathbf{P}$. Conversely, any norm for the initial perturbations also implies a covariance matrix: if the initial norm is defined by a matrix $\mathbf{S}$ via $|\phi|_0^2 = \phi^*\mathbf{S}\phi$, then the implied covariance matrix for initial perturbations is $\mathbf{P} = \mathbf{S}^{-1}$. A natural question is what are the characteristics of perturbations implied by the energy norm. We will call these "energy" perturbations.

For quasigeostrophic flows, the total energy norm is obtained by choosing $\mathbf{S} = -\nabla^2$ and $\mathbf{P} = -\nabla^{-2}$, where $\nabla^2$ is the discrete Laplacian operator based on boundary conditions $\phi_z = 0$ at $z = 0, 1$, as described in the appendix. The eigenvalues and eigenvectors of $\mathbf{P}$ are

$$\lambda_m^2 = \{k^2 + 2n^{-2}[1 - \cos((m-1)\pi/n)]\}^{-1}, \quad m = 1, \ldots, n,$$

and

$$\mathbf{P}_m = \cos((m-1)\pi\mathbf{z}), \quad m = 1, \ldots, n,$$

where the vector $\mathbf{z}$ contains the grid-level heights $z_j = (j - 1/2)/n$ $(j = 1, \ldots, n)$ and the cosine is taken element by element.

Figure 8a shows a typical energy perturbation; that is, a perturbation drawn randomly from a Gaussian distribution with zero mean and covariance $\mathbf{P} = -\nabla^{-2}$. (This sampling is accomplished by taking $\boldsymbol{\phi} = \Sigma_{m=0}^{n-1} \lambda_m(a_m + ib_m)\mathbf{p}_m$, where the $a_m$ and $b_m$ are mutually independent Gaussian random variables with zero mean and unit variance.) Although most of the variance resides in the largest vertical scales (consistent with eigenvalues and eigenvectors of $\mathbf{P}$), significant variability on finer vertical scales is also apparent owing to the relatively slow decrease of $\lambda_m$ with $m$. The finescale structure clearly distinguishes this "energy" perturbation from the much smoother structure of the upper trough shown in Fig. 3a.

In the previous section, we argued that perturbations such as the upper trough were characterized by small PV variance in the interior troposphere relative to the upper and lower boundaries. Since PV perturbations are related to streamfunction through $\mathbf{q} = \nabla^2\boldsymbol{\phi}$, the covariance matrix for the PV of the energy perturbations is $\mathbf{Q} = \nabla^2\,\mathbf{P}\,\nabla^2 = -\nabla^2$; the eigenvectors of $\mathbf{Q}$ are thus identical to those of $\nabla^{-2}$ and the eigenvalues are $\lambda_m^{-2}$. The leading eigenvector $\mathbf{p}_n$ of $\mathbf{Q}$, which appears in Fig. 8b, oscillates from one grid level to the next and has maximum amplitude in the midtroposphere. The energy norm thus favors vertical structure in PV at the

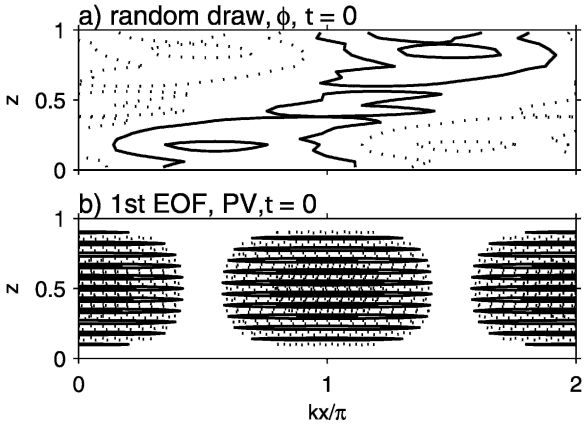


FIG. 8. Perturbations implied by the energy norm. (a) The streamfunction for a perturbation drawn randomly from $N(0, \mathbf{P})$ with $\mathbf{P} = \mathbf{S}^{-1} = -\nabla^{-2}$. (b) The leading eigenvector of the PV covariance matrix, $\mathbf{Q} = \nabla^2\mathbf{P}\nabla^2$. Contours are shown at 1/4 and 3/4 the maximum value of the field, with negative values dotted.

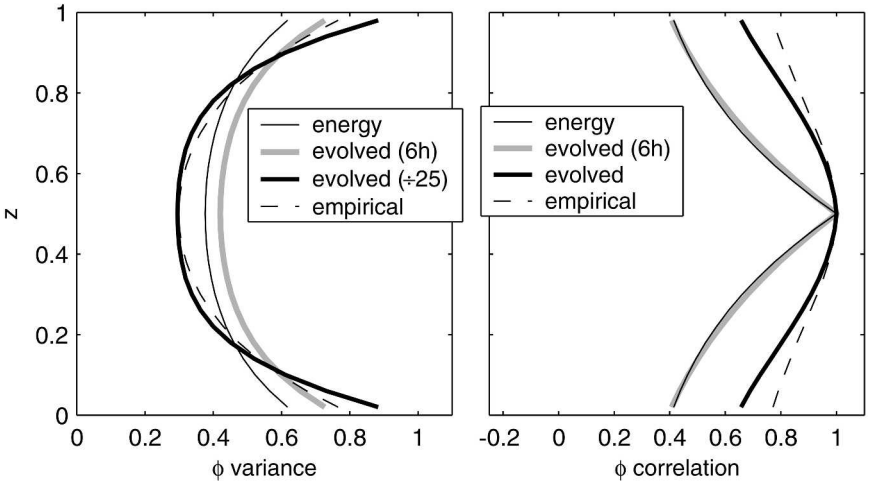


FIG. 9. (left) Streamfunction variance as a function of height and (right) the vertical autocorrelation of streamfunction with its value at $z = 1/2$. Results are shown for four covariance matrices: that implied by the energy norm (solid lines), the energy covariances evolved over 6 and 48 h (thick gray and thick solid, respectively), and the empirical covariances given by (8) (dashed). Note that the 48-h evolved variance has been divided by a factor of 25 for display and that the vertical correlations from the energy covariance and from the 6-h evolved covariance differ by less than the width of the thick gray line. The vertical correlations are computed for constant $x$.

finest resolved vertical scales. This provides another interpretation of the energy SV structure.

## 7. Vertical structure of typical perturbations and analysis errors

We have shown that the SVs based on the empirical covariance norm provide a more efficient decomposition of the upper trough and a simpler description of its dynamics than do the energy SVs. The key issue that remains is whether initial perturbations and analysis errors do, in fact, have relatively smooth vertical structure and limited interior PV, like the upper trough and as represented in the empirical covariances (8). In this section, we first review the dynamics that tend to remove vertical structure as quasigeostrophic perturbations evolve in shear. We then review empirical evidence, both from observations of cyclogenesis and from various surrogates for analysis errors, for the vertical structure of initial perturbations. While the situation is fairly clear for cyclogenetic perturbations, we warn the reader at the outset that available information about analysis errors is circumstantial and hardly conclusive.

### *a. Dynamical influences*

The dynamical evolution of perturbations, during which certain perturbations grow while others decay, is a fundamental process that imposes characteristic structure on the perturbations. One way to measure the influence of this process is to consider the covariance matrix of perturbations evolved to $t = \tau$, which is given by $\mathbf{P}(\tau) = \mathbf{M}\mathbf{P}(0)\mathbf{M}^*$.

Figure 9a displays the variance of $\phi$ as a function of height for three covariance matrices: the empirical covariance of section 5, the energy covariance, and the evolved covariance $\mathbf{P}(\tau)$ beginning from the energy covariance. In addition to producing the overall growth of the perturbation variance, the dynamics also decreases the variance in the midtroposphere relative to that at either the surface or the lid. The evolved variances resemble those from the empirical covariance, rather than the initial energy covariance.

Figure 9b shows the correlation of $\Re(\phi(z))$ at each level with its value at $z = 1/2$, based on the same three covariance matrices. It is evident from the broader evolved vertical correlations that the dynamics acts to produce deep, smooth perturbations and to remove fine structure from the interior of the troposphere. [The evolved perturbations tend to tilt westward with height as well (not shown).] As for the variances, the evolved correlations more closely resemble those from the empirical covariance than those from the energy covariance.

The leading energy SV also exhibits this kind of evolution. As can be seen in Figs. 2a,b, the vertical scales increase and the maximum amplitudes shift from the midtroposphere to the boundaries as the SV evolves. Energy SVs from global forecast models behave in much the same fashion (e.g., Buizza and Palmer 1995), as do perturbations drawn randomly from a Gaussian distribution with the energy covariance and evolved in a turbulent quasigeostrophic flow (Snyder et al. 2003).

In all these cases, the time scale for evolution away from the midtroposphere and to larger vertical scales is of the order of a day for typical tropospheric parameters.

In terms of PV, the perturbations grow at the upper and lower boundaries where they can interact with the basic-state PV gradients, while the perturbation PV is simply advected by the basic-state shear in the interior. Thus, over time, the boundary PV increases relative to that in the interior and the streamfunction becomes smoother and deeper in the vertical. Snyder et al. (2003) have shown that concentration of perturbation PV where basic-state PV gradients are large is also pronounced in complex, turbulent quasigeostrophic flows. The empirical covariances specified in section 5 represent an intermediate stage of this dynamical evolution in which the boundary and interior PV make equal contributions to the domain-integrated potential enstrophy. The dynamics can also be described, broadly equivalently, in terms of the conservation of wave activity as perturbations propagate from regions of small PV gradient to regions of larger gradients (Buizza and Palmer 1995; Morgan 2001) or in terms of the "unshielding" and vertical propagation of perturbations (Hoskins et al. 2000).

Since these dynamics most affect evolved perturbations, the extent of the dynamical influence on the vertical structure of cyclogenetic perturbations or analysis errors is not obvious a priori. For example, in the case of cyclogenesis, initial perturbations may be produced not by the adiabatic dynamics but rather by the injection of PV perturbations into the midtroposphere by latent heat release or other diabatic effects. Analysis errors are influenced by dynamics through the use of a background forecast in the assimilation, but assimilation of observations also clearly influences the structure of analysis errors. Thus, to evaluate whether dynamical influences are important in conditioning the structure of initial disturbances, we turn next to reviewing evidence concerning the vertical structure of cyclogenetic perturbations and analysis errors.

### b. Observations of cyclogenesis

The most commonly observed scenario for surface cyclogenesis is a deep, pre-existing upper trough above a surface baroclinic zone (Pettersen and Smebye 1971). It is also the basis for schematic models of surface cyclogenesis (Hoskins et al. 1985, their Fig. 21) and finds its simplest expression in the upper trough given by (4) and used in the previous examples.

Since the perturbation does not have fine vertical structure and has relatively little amplitude or PV in the midtroposphere, this scenario reflects the dynamical influences just discussed and is most consistent with the empirical covariance. Case studies of cyclogenesis using PV inversions also support this view as they reveal PV perturbations in the upper troposphere to be crucial while PV perturbations in the midtroposphere are not always important or even present (Davis 1992; Rotunno and Bao 1996). More generally, observations indicate that PV gradients are weak and PV anomalies are small in the interior of the troposphere, away from the surface and tropopause (Morgan and Nielsen-Gammon 1998). Furthermore, observations also indicate that cyclogenesis precursors are often localized coherent tropopause vortices that possess little, if any, tilt in the vertical (Hakim 2000).

### c. Surrogates for analysis errors

Our knowledge of analysis errors is inherently limited since all observations are contaminated by errors and, moreover, almost all available observations are utilized in operational analyses and so cannot provide independent information about the analyses' quality. Here we consider three surrogates for the errors of operational analyses: (i) analysis errors in experiments with simplified models and simulated observations, where the true state is known and analysis errors may be calculated directly; (ii) differences between operational analyses; and (iii) differences between observations and short-range background forecasts used in assimilation schemes. As will be discussed in what follows, each of these are imperfect substitutes for analysis errors.

Data assimilation experiments with simulated observations suggest that, owing to the use of a background forecast in the assimilation process, a significant dynamical signal remains in the error structures even after observations are assimilated. Hamill et al. (2002) demonstrate this in a quasigeostrophic model using simulated observations and a three-dimensional variational assimilation scheme. They find that the analysis errors reflect the dynamical influences in that they tend to be deep, with little vertical structure, and have maximum amplitude near the tropopause. Hamill et al. (2003) find similar results in a simplified general circulation model using an ensemble Kalman filter. Because they are based on observations taken from numerical simulations, rather than from the real atmosphere, these experiments cannot fully represent all error sources that affect analysis errors. They nevertheless demonstrate that the assimilation process itself need not inherently mask the dynamical influences.

Differences between operational analyses are a particularly convenient surrogate. They have been used by Palmer et al. (1998) and Hakim (2005) to investigate the horizontal and vertical structure of analysis errors, respectively. Analysis differences nevertheless differ from analysis errors because operational analyses utilize many of the same observations and are based on forecast models and assimilation schemes that may have similar deficiencies.

We have calculated the vertical structure of analysis

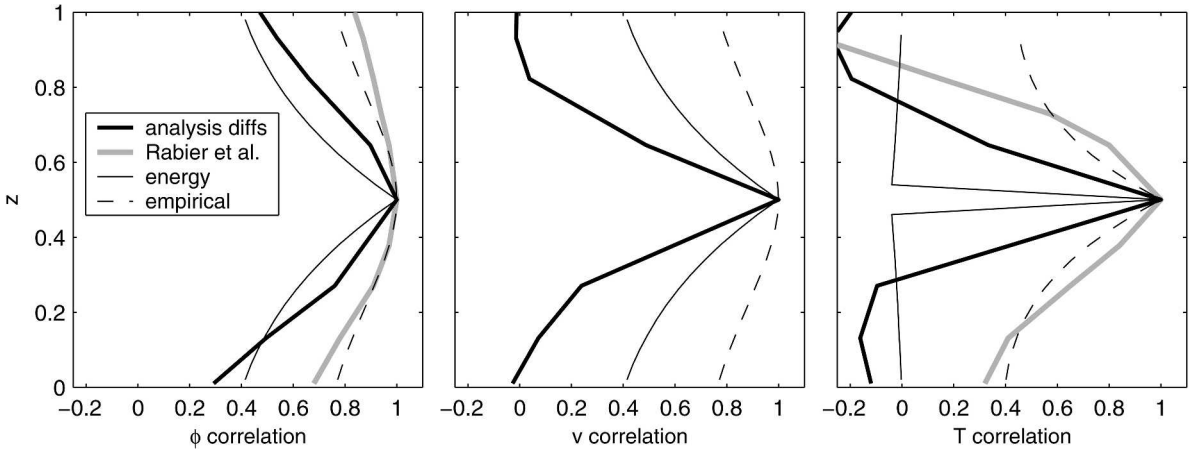


FIG. 10. (left) Vertical autocorrelations of streamfunction, (center) $v$, and (right) $T$ based on differences of operational analyses (thick lines). Correlations of each level with that at 500 hPa are shown, together with the same correlations based on the energy covariance (thin lines) and the empirical covariance (dashed). The analysis differences are calculated for wavenumber 9 at 40°N latitude. (left), (right) Vertical autocorrelations (gray lines) at total spherical wavenumber 10 from Rabier et al. (1998, their Figs. 9a,c).

differences using global operational analyses[2] from the National Centers for Environmental Prediction, Fleet Numerical Meteorology and Oceanography Center, and the U. K. Meteorological Office. At each analysis time, we compute the mean of the analyses and the difference of the individual analyses from the mean. Given a vertical profile of analysis differences along a latitude circle, we calculate the Fourier transform at each level and then, given a large sample, form the covariance matrix (among levels) for each zonal wavenumber. One could also consider the vertical covariances at a specific horizontal location, but only covariances at a given wavenumber are presented here to facilitate comparison with preceding results from the Eady problem, which also pertain to a single wavenumber. We will examine vertical correlations for wavenumber 9 at 45°N latitude, since the nondimensional wavenumber $k = 2.5$ used in the previous examples corresponds to a wavenumber of roughly 10 in midlatitudes.

The computed analysis differences yield the vertical autocorrelation for streamfunction $\phi$, meridional velocity $v$, and temperature $T$ at 500 hPa shown in Fig. 10. For comparison with the vertical correlations from the energy and empirical covariances, the pressure levels for the analysis-difference correlations are assigned heights based on the standard atmosphere and those heights are then rescaled by a constant factor so that 500 hPa corresponds to $z = 0.5$.

[2] The analyses are transformed from native grids to latitude–longitude grids on pressure surfaces at the operational centers, and are made available to the University of Washington. Data from 1000, 850, 700, 500, 400, 300, 250, and 200 hPa were used in this study, as these were the pressure surfaces available for all three analyses.

For $\phi$, the vertical correlations estimated from analysis differences are closer to those from the energy covariance than those from the empirical covariance. For $v$, the estimated correlations are significantly weaker than those from either of the covariance models. In terms of $T$, the correlation from the energy covariance is very sharp, while both the estimated correlations and those from the empirical covariance are broader. Notice that the $T$ correlations from the energy covariance are singular in the limit that the number of levels $n \to \infty$, and the width of the peak shown in Fig. 10 is limited only by the grid spacing.

The final surrogate for analysis errors we consider are short-range forecast errors. For sufficiently short forecasts, these will of course resemble analysis errors. To illustrate this, Fig. 9 shows variances and vertical correlations for the energy covariances evolved to $t = \tau/8$ (corresponding to a dimensional time of 6 h) rather than $t = \tau$. The evolved covariances for this shorter period of evolution are barely distinguishable from the energy covariances, indicating that, for midlatitude synoptic-scale flows, 6-h forecast errors should retain a significant resemblance to the analysis errors from which they originated. Of course, forecast errors at smaller scales may evolve more quickly, particularly in flows with conditional instability and moist convection (see e.g., Zhang et al. 2003).

Short-range forecast errors are not significantly larger than analysis errors and thus cannot be estimated by comparing the forecast against a verifying analysis. Their homogeneous, isotropic component, however, can be estimated from the differences between the forecasts and observations (following Hollingsworth and Lönnberg 1986) or, with very similar results, from differences between forecasts. Rabier et al. (1998) use the latter method to estimate short-range forecast error co-

variances. Their vertical correlations with 500 hPa at total spherical wavenumber 10 (see their Figs. 9a,c) appear as the gray lines in Fig. 10. Aside from their opposite sign for $T$ near the climatological tropopause (which we believe arises from the lack of a flexible tropopause in the Eady problem), these vertical correlations resemble those from the empirical covariance. The correlations estimated by Rabier et al. are also much broader than either those estimated from analysis differences or those implied by the energy covariance.

Clearly, the surrogates for analysis error are insufficient to distinguish between the empirical covariances and the energy covariances: The covariances estimated from forecast differences resemble the empirical covariances, while those estimated from analysis differences agree best with the energy covariances, although the vertical $T$ correlations based on the energy covariances are much sharper than either estimate. We conclude that analysis errors that are deep and lack fine vertical structure, consistent with the influence of the dynamics and as we assumed in developing the empirical covariances, are as plausible as those implied by the energy norm.

## 8. Summary and discussion

We have considered a typical initial condition for cyclogenesis, consisting of an upper level trough above a surface baroclinic zone, and examined its decomposition into SVs based on the total energy norm. We have also argued that this example may be relevant to the evolution of forecast errors. For simplicity, the calculations presented are quasigeostrophic and two dimensional, assume the Eady basic state with constant vertical shear, and pertain to a single zonal wavenumber.

The evolution of the upper trough is easily understood in terms of potential vorticity and its associated induced flows (e.g., Hoskins et al. 1985); yet in terms of energy SVs the evolution arises from a complex superposition of rapidly growing and decaying perturbations, each of which exhibits dynamics distinct from that of the original perturbation. These differences in dynamics are linked to differences in vertical structure at the initial time: the upper trough has smooth structure, decaying slowly from the tropopause downward, whereas almost all the initial energy SVs (particularly those that grow rapidly) are highly structured in the vertical and have maximum amplitude in the midtroposphere.

The structure and evolution of the SVs can be reconciled with those of our chosen, typical perturbation by explicitly incorporating information about the likelihood of initial perturbations. Such information can be included in the calculation of SVs by assuming the initial perturbations to be Gaussian random variables with known statistics. The natural initial norm is then defined by the inverse of the perturbations' covariance matrix and measures the (negative) log likelihood of any initial perturbation. We have proposed an empirical covariance norm based on the notion that typical cyclogenetic perturbations or analysis errors have only limited potential vorticity in the interior of the troposphere. Singular vectors based on this norm provide a particularly economical description of the evolution of the upper trough and do not suffer from the strong cancellation of PV found for the energy SVs.

The structure of the energy SVs can also be understood by viewing the problem in terms of the relation of the initial norm and the covariance matrix of initial perturbations. Just as specifying a covariance matrix defines a norm, specifying an initial norm implies a covariance matrix for the initial perturbations. In our simple example, the covariance matrix for streamfunction implied by the energy norm is $\nabla^{-2}$, the inverse of the discrete Laplacian. For PV, the implied covariance matrix is $\nabla^2$ so that most of the PV variance resides in the finest vertical scales. Consistent with this, the initial energy SVs are finely structured in the vertical.

The question then reduces to determining the vertical structure of cyclogenetic perturbations or analysis errors. Section 7 reviewed how the dynamics of quasigeostrophic disturbances in vertical shear lead generically to smoother vertical structure as the disturbances evolve, and also reviewed a variety of empirical evidence concerning the vertical structure of cyclogenetic perturbations and analysis errors. For cyclogenetic perturbations, observational evidence favored the empirical covariances. The evidence available from various surrogates for analysis errors, however, was less conclusive. Analysis differences resembled the perturbations implied by the energy covariances most closely, while short-range forecast errors and analysis errors from data-assimilation experiments with simulated observations were more similar to the empirical covariances. The vertical structure of analysis errors thus remains an outstanding issue with important implications for the choice of norm in SV calculations related to predictability studies and ensemble forecasting.

An important limitation of this study is that we have not considered the horizontal structure of perturbations or errors. Like the vertical structure, the horizontal structure of analysis errors is poorly known. Palmer et al. (1998) show that the horizontal kinetic-energy spectrum of a limited sample of analysis differences is nearly flat for total wavenumbers between 0 and 40 on the sphere. As they note, such a spectrum is consistent with the covariances implied by the energy norm. At the same time, Hollingsworth and Lönnberg (1986) find that the isotropic component of 6-h forecast errors (which we have argued may resemble analysis errors) has a kinetic energy spectrum that peaks at wavenumbers less than 20 and decays for larger wavenumbers. Similarly, Hakim (2005) found a peak between zonal wavenumbers 10 and 15 in both analysis and 12-h forecast errors for the meridional wind at 40°N.

Regardless of the horizontal structure, it is clear the vertical structure of perturbations, on which we have concentrated here, has a substantial influence on their behavior. In particular, Snyder and Joly (1998) show that when perturbations are constrained to have zero PV in the troposphere, the leading energy SV on a growing baroclinic wave evolves toward synoptic scales from the largest horizontal scales, rather than upscale from subsynoptic scales as is usual for energy SVs (Buizza and Palmer 1995). This constraint on the perturbation PV is much like that implied by the empirical covariances proposed in section 5. The importance of large-scale analysis differences to subsequent forecast differences has also been found in experiments with global forecast models (Miguez-Macho and Paegle 2000).

Finally, we stress how SVs for the energy norm or the empirical covariance norm lead to divergent views of the development of the upper trough, and by extension, of cyclogenesis and the origins of forecast errors. The upper trough has a small projection on the leading energy SVs. The leading energy SVs, however, grow very rapidly so that after 48 h the leading four SVs account for over 90% of the energy of the evolved trough. Thus, when viewed through the energy SVs, the evolution of the upper trough arises from a small seed, given by the projection on the leading SVs, that grows rapidly and changes its vertical structure dramatically over 48 h. Projecting onto the empirical covariance SVs, in contrast, emphasizes slower growth and perturbations associated with the tropopause and surface and having smoother vertical structure that persists throughout the time interval.

*Acknowledgments.* We are indebted to Professor Clifford Mass (University of Washington) for providing access to operational analyses for use in the analysis-error portion of the study. Comments from Professor David Muraki (Simon Fraser University) and Richard Rotunno (NCAR), as well as from the reviewers, led to significant improvements in the manuscript. GJH acknowledges support from the National Science Foundation through Grants ATM-0228804 and ITR-0205648, and from National Oceanic and Atmospheric Administration through CSTAR Grant NA 17RJ1232.

## APPENDIX

### Vertical Discretization

Using $n$ vertical levels, we discretize (1) with $\phi_j$ and $q_j$ on grid points $z_j = (j - 1/2)/n$ staggered by a distance $(1/2)n$ (i.e., half the grid interval $n^{-1}$) from the boundaries at $z = 0, 1$. The potential temperature $\theta_j$ is defined at the unstaggered levels $\hat{z}_j = j/n$.

The PV and potential temperature are related to streamfunction by centered differences,

$$q_j = n^2(\phi_{j+1} - 2\phi_j + \phi_{j-1}) - k^2\phi_j, \quad j = 1, \ldots, n; \tag{A1}$$

$$\theta_j = n(\phi_{j+1} - \phi_j), \quad j = 0, \ldots, n. \tag{A2}$$

The governing Eqs. (1a), (1b) in discrete form are

$$\partial_t q_j = -ik(z_j - 1/2)q_j, \quad j = 1, \ldots, n, \tag{A3a}$$

$$\partial_t \theta_j = -ik(\hat{z}_j - 1/2)\theta_j + ik(\phi_{j+1} + \phi_j)/2, \quad j = 0, n. \tag{A3b}$$

Equations (A3a) and (A3b), together with (A1), and the boundary conditions given for $j = 0$, $n$ by (A2) constitute $n + 2$ equations for $\phi_j$, $j = 0, \ldots, n + 1$. Notice, however, that $\phi_0$ and $\phi_{n+1}$ represent the streamfunction at "ghost levels" one-half grid level below the surface and above the lid, respectively.

Values of $\phi$ outside the physical domain may be eliminated by introducing on the first and last interior levels a generalized PV $\tilde{q}$, given by

$$\tilde{q}_1 \equiv q_1 + n\theta_0 = n^2(\phi_2 - \phi_1) - k^2\phi_1; \tag{A4}$$

$$\tilde{q}_n \equiv q_n - n\theta_n = n^2(\phi_{n-1} - \phi_n) - k^2\phi_n. \tag{A5}$$

When we refer to the discretized version of the Laplacian $\nabla^2$, we mean the rhs of (A4), (A5), and (A1) for $j = 2, \ldots, n - 1$. Notice that this is the form of $\nabla^2$ that would be obtained for homogeneous boundary conditions $\partial_z\phi = 0$ on $z = 0, 1$, consistent with the incorporation of the boundary $\theta$ into the interior PV in (A4) and (A5). An evolution equation for $\tilde{q}$ on the first and last interior levels can be formed by combining (A3a) at $j = 1$, $n$ with (A3b), which yields

$$\partial_t \tilde{q}_1 = -ik[(z_1 - 1/2)q_1 + n((\hat{z}_0 - 1/2)\theta_0 - \phi_1/2 - \phi_0/2)]$$

$$= -ik[(z_1 - 1/2)\tilde{q}_1 - n\phi_1]; \tag{A6}$$

$$\partial_t \tilde{q}_n = -ik(z_n\tilde{q}_n + n\phi_n). \tag{A7}$$

Values of $\phi$ outside the domain are again eliminated.

The results in this paper take $\phi_j$, $j = 1, \ldots, n$ to be the elements of the state vector $\phi$ and are based on solving (A4)–(A6) together with (A1) and (A3a) for $j = 2, \ldots, n - 1$. The incorporation of the boundary potential temperature perturbations into the interior PV in (A4) and (A5) is the discrete equivalent of replacing the potential temperature on rigid boundaries by a sheet of PV in the continuous problem (see Bretherton 1966). This generalization of PV pertains both to the perturbations ($\tilde{q}_j$, $j = 1, n$) and to the basic state; the terms proportional to $ik\phi_j$ on the rhs of (A6) and (A7) represent the advection of meridional gradient of the basic-state generalized PV, which arises from the basic-state gradient of potential temperature.

The energy of a perturbation is taken to be

$$|\boldsymbol{\phi}|^2 = \sum_{j=1}^{n-1} (\theta_j^2 + k^2\phi_j^2).$$

To find the elements of the corresponding matrix $\mathbf{S}$ such that $|\boldsymbol{\phi}|^2 = \boldsymbol{\phi}^*\mathbf{S}\boldsymbol{\phi}$, we use the definition (A2) of $\theta_j$

and expand the squares. The main diagonal of **S** corresponds to the coefficients of $\phi_j^2$ terms, while the first upper and first lower diagonals each contain the coefficients of the $\phi_j\phi_{j+1}$ terms divided by two. Thus, the first and last elements on the main diagonal are $n^2 + k^2$, the other main diagonal elements are $2n^2 + k^2$, and the elements in the first upper and first lower diagonals are $-n^2$. These are precisely the negative of the elements of the discretized $\nabla^2$ defined by (A4), (A5), and (A1) for $j = 2, \ldots, n - 1$.

## REFERENCES


Barkmeijer, J., M. van Gijzen, and F. Bouttier, 1998: Singular vectors and estimates of the analysis error covariance metric. *Quart. J. Roy. Meteor. Soc.,* **124,** 1695–1713.

Bretherton, F. P., 1966: Critical layer instability in baroclinic flows. *Quart. J. Roy. Meteor. Soc.,* **92,** 325–334.

Buizza, R., and T. N. Palmer, 1995: The singular-vector structure of the atmospheric general circulation. *J. Atmos. Sci.,* **52,** 1434–1456.

——, J. Tribbia, F. Molteni, and T. Palmer, 1993: Computation of optimal unstable structures for a numerical weather prediction model. *Tellus,* **45A,** 388–407.

Davis, C. A., 1992: A potential vorticity diagnosis of the importance of initial structure and condensational heating in observed extratropical cyclogenesis. *Mon. Wea. Rev.,* **120,** 2409–2428.

Eady, E. T., 1949: Long waves and cyclone waves. *Tellus,* **1,** 33–52.

Ehrendorfer, M., and J. J. Tribbia, 1997: Optimal prediction of forecast error covariances through singular vectors. *J. Atmos. Sci.,* **54,** 286–313.

Farrell, B. F., 1989: Optimal excitation of baroclinic waves. *J. Atmos. Sci.,* **46,** 1193–1206.

——, 1990: Small error dynamics and the predictability of flows. *J. Atmos. Sci.,* **47,** 2409–2416.

Gelaro, R., R. Buizza, T. N. Palmer, and E. Klinker, 1998: Sensitivity analysis of forecast errors and the construction of optimal perturbations using singular vectors. *J. Atmos. Sci.,* **55,** 1012–1037.

Gill, A. E., 1982: *Atmosphere–Ocean Dynamics.* Academic Press, 662 pp.

Hakim, G. J., 2000: Climatology of coherent structures on the extratropical tropopause. *Mon. Wea. Rev.,* **128,** 385–406.

——, 2005: Vertical structure of midlatitude analysis and forecast errors. *Mon. Wea. Rev.,* **133,** 567–578.

Hamill, T. M., C. Snyder, and R. E. Morss, 2002: Analysis-error statistics of a quasigeostrophic model using three-dimensional variational assimilation. *Mon. Wea. Rev.,* **130,** 2777–2790.

——, ——, and J. S. Whitaker, 2003: Ensemble forecasts and the properties of flow-dependent analysis-error covariance singular vectors. *Mon. Wea. Rev.,* **131,** 1741–1758.

Hollingsworth, A., and P. Lönnberg, 1986: The statistical structure of short-range forecast errors as determined from radiosonde data. Part I: The wind field. *Tellus,* **38A,** 111–136.

Hoskins, B. J., M. E. McIntyre, and A. W. Robertson, 1985: On the use and significance of insentropic potential vorticity maps. *Quart. J. Roy. Meteor. Soc.,* **111,** 877–946.

——, R. Buizza, and J. Badger, 2000: The nature of singular vector growth and structure. *Quart. J. Roy. Meteor. Soc.,* **126,** 1565–1580.

Houtekamer, P. L., 1995: The construction of optimal modes. *Mon. Wea. Rev.,* **123,** 2888–2898.

Kim, H. M., and M. Morgan, 2002: Dependence of singular vector structure and evolution on the choice of norm. *J. Atmos. Sci.,* **59,** 3099–3116.

Lacarra, J.-F., and O. Talagrand, 1988: Short-range evolution of small perturbations in a barotropic model. *Tellus,* **40A,** 81–95.

Lorenz, E. N., 1965: A study of the predictability of a 28-variable atmospheric model. *Tellus,* **17,** 321–333.

Miguez-Macho, G., and J. Paegle, 2000: Sensitivity of a global forecast model to initializations with reanalysis datasets. *Mon. Wea. Rev.,* **128,** 3879–3889.

Morgan, M., 2001: A potential vorticity and wave activity diagnosis of optimal perturbation evolution. *J. Atmos. Sci.,* **58,** 2518–2544.

——, and J. Nielsen-Gammon, 1998: Using tropopause maps to diagnose midlatitude weather systems. *Mon. Wea. Rev.,* **126,** 2555–2579.

Mukogawa, H., and T. Ikeda, 1994: Optimal excitation of baroclinic waves in the Eady model. *J. Meteor. Soc. Japan,* **72,** 499–513.

Palmer, T. N., R. Gelaro, J. Barkmeijer, and R. Buizza, 1998: Singular vectors, metrics, and adaptive observations. *J. Atmos. Sci.,* **55,** 633–653.

Pettersen, S., and S. Smebye, 1971: On the development of extratropical cyclones. *Quart. J. Roy. Meteor. Soc.,* **97,** 457–482.

Rabier, F., A. McNally, E. Andersson, P. Courtier, P. Unden, J. Eyre, A. Hollingsworth, and F. Bouttier, 1998: The ECMWF implementation of three-dimensional variational assimilation (3D-Var). II: Structure functions. *Quart. J. Roy. Meteor. Soc.,* **124,** 1809–1829.

Rotunno, R., and M. Fantini, 1989: Petterssen's "type B" cyclogenesis in terms of discrete, neutral Eady modes. *J. Atmos. Sci.,* **46,** 3599–3604.

——, and J.-W. Bao, 1996: A case study of cyclogenesis using a model hierarchy. *Mon. Wea. Rev.,* **124,** 1051–1066.

Snyder, C., and A. Joly, 1998: Development of perturbations within a growing baroclinic wave. *Quart. J. Roy. Meteor. Soc.,* **124,** 1961–1983.

——, T. M. Hamill, and S. Trier, 2003: Linear evolution of forecast error covariances in a quasigeostrophic model. *Mon. Wea. Rev.,* **131,** 189–205.

Zhang, F., C. Snyder, and R. Rotunno, 2003: The influence of moist convection on the limits of mesoscale predictability. *J. Atmos. Sci.,* **60,** 1173–1185.